Journal of the European Ceramic Society 22 (2002) 2081–2092

www.elsevier.com/locate/jeurceramsoc

Rheological properties of PZT suspensions for stereolithography

Olivier Dufaud[a], Philippe Marchal[b], Serge Corbel[a,*]

[a]*Département de Chimie Physique des Réactions (DCPR), UMR 7630 CNRS-INPL Groupe ENSIC, 1 rue Grandville, BP 451-54001 Nancy Cedex, France*

[b]*Centre de Genie chimique des Milieux rhéologiquement Complexes (GEMICO), Groupe ENSIC, 1 rue Grandville, BP 451-54001 Nancy Cedex, France*

Received 27 June 2001; received in revised form 11 February 2002; accepted 24 February 2002

Abstract

The study of the rheological behaviour of PZT suspensions is essential to a better understanding of piezocomposites fabrication through stereolithography process. Research concerns the influence of fillers contents, surfactant doses, temperature and resin nature on suspensions rheological behaviour. They have led to the choice of two photosensitive suspensions suitable for stereolithography purpose; which use depends on the fillers content. Furthermore, the stereolithography process has been modified owing to the balance between suspensions rheological and photochemical properties in order to shape piezoelectric ceramics. Thanks to these improvements, PZT ceramics/polymer composites dedicated to transducers and medical imaging applications have been fabricated.

Keywords: Suspensions; Rheology; PZT; Piezoelectric properties; Stereolithography; $Pb(Zr,Ti)O_3$

1. Introduction

Piezoelectricity is defined as the ability of certain classes of crystalline materials to produce a voltage proportional to the mechanical pressure applied to their boundaries. Conversely, when an electrical field is applied, their crystalline structure changes shape, producing dimensional changes in the material.

Ceramics as lead zirconate titanate $Pb(Zr,Ti)O_3$ (PZT) are widely used piezoelectric materials, due to their high dielectric (relative dielectric constant κ) and piezoelectric properties, such as the electromechanical coupling coefficient ($k = \{\text{energy stored/energy applied}\}^{1/2}$), the charge coefficient (d_{33} = strain developed/applied field) and low electrical losses ($\tan\delta \leqslant 0.05$).[1,2] However an electromechanical transducer, for instance, might also require a low density and high mechanical flexibility, which is not the case in PZT ceramics. Consequently, in the past two decades, the stress was put on PZT ceramic/polymer composites.[3,4] Their advantages lie in the mixing of the high piezoelectric properties of the ceramics with the mechanical and acoustical benefits of the polymer (low acoustic impedance Z_a). Moreover the flexibility of these composites allows their positioning on concave/convex surfaces.

Applications for such piezoelectric materials are numerous and include microphones, strain or pressure gauges, hydrophones, microtransducers and ultrasound medical imaging. In this work, the manufactured parts are piezocomposites with 1–3 connectivity which are well suited for biomedical imaging.[5,6] The connectivity describes the structural arrangement of the composite phases, generally the ceramic and the polymer. For a bicomponent there are 16 connectivity patterns among which are the most studied forms: 0–3, 2–2, 3–2, 1–3...[7] In a 1–3 piezocomposite, piezoelectric rods oriented in one direction z are drowned in a polymer self-connected in three dimensions.[8]

A large number of forming methods have already been demonstrated : usual processing techniques as ''dice and fill'' or ''pick and place'', and more recently injection moulding, fused deposition of ceramics or fibre processing.[9–11] In this context, the fabrication of such composites by stereolithography seems to be promising.

Stereolithography is a rapid prototyping process for three-dimensional polymer parts fabrication[12,13] (Fig. 1). In this technology, a computer-controlled laser beam

* Corresponding author.
E-mail address: serge.corbel@ensic.inpl-nancy.fr (S. Corbel).

0955-2219/02/$ - see front matter
PII: S0955-2219(02)00036-5

Nomenclature

κ	relative dielectric constant
k	electromechanical coupling coefficient
d_{33}	piezoelectric charge coefficient
$\tan\delta$	dielectric losses
Z_a	acoustic impedance
d_x	xth percentile particle size
τ	shear stress
$\dot{\gamma}$	shear rate
η	apparent viscosity
$G*$	complex modulus
G'	storage modulus
G''	loss modulus
ω	frequency
γ	strain
δ	phase angle
d	sphere diameter
u_t	terminal velocity
ρ	density
η	high-shear Newtonian limit
η_0	low-shear Newtonian limit
K, m	Cross parameters
k	consistency
n	power-law index
v	scrapper rate
e	layer thickness
Φ	volume fraction of fillers
Φ_0	theoretical packing factor
β	effective packing factor
θ	bonds angle
$[\eta]$	intrinsec viscosity
b	thickness of the absorbed dispersant layer
N	number of segments of a carbons linear chain
l	length of a C-C bond
$\sqrt{\overline{r}^2}$	average quadratic length of a molecule
A	pre-exponential factor
E_a	activation energy
T	temperature
HLB	hydrophilic and lipophilic balance

(351–365 nm, ionised argon) induces polymerisation of a liquid monomer into a solid polymer. The succession of photopolymerised layers, thanks to an elevator (Charlyrobot motor) leads to the formation of a 3D part. This process was modified to allow 3D ceramic green parts fabrication from ceramic suspensions.[14,15]

The advantages of stereolithography are its flexibility in manufacturing composites with different geometries and dimensions, due to computer aided design (CAD), its accuracy and its quickness. Thus, the design flexibility of this process allows an accurate fit of rods placement, which determined the PZT volume fraction and consequently the efficiency of the emission and transmission modes of the transducer. The fine control of its thickness permits the adjustment of its resonant frequency.

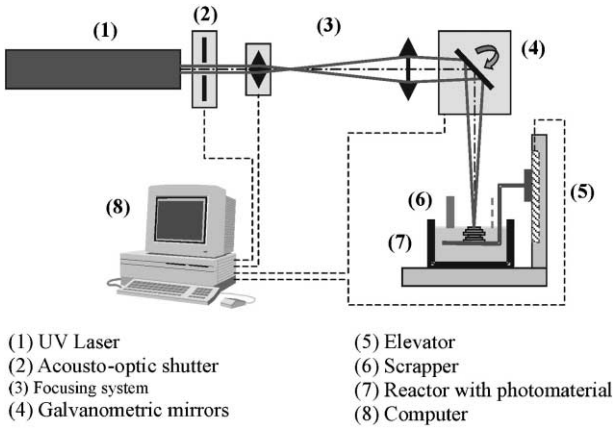

Fig. 1. Scheme of the stereolithography process.

The study of ceramic suspensions rheological behaviour is essential for stereolithography adjustment.[16,17] First of all, the dispersions must be homogeneous, stable and well dispersed. The sedimentation must also be consistent with our fabrication rate to avoid a progressive decrease in PZT content of the green parts. Thus, the influence of dispersant nature and concentration was studied in this aim.

Another restraint of the processing of PZT by stereolithography is the low cure depth of these suspensions, which implies the spreading of very thin photomaterial layers (usually 20 μm) to ensure their binding. So, the adjustment of the binder formulation is a compulsory stage in this work. It also allows the improvement of spreading dynamic.

Different kinds of scrappers were used to speed up monomer spreading and control the layer thickness. Then, it is advantageous to use dispersions with appropriate rheological behaviour, especially a shear-thinning one.

On the one hand, in order to improve green parts sintering and ensure good piezoelectric properties, the fillers content of the suspensions must be rather high. On the other hand, an increase in PZT concentration lowers the polymerisation depth, which is unfavourable to object cohesion. As a consequence, the influence of ceramic content on suspensions rheology was investigated.

In this paper, the importance of dispersion viscoelasticity is also pointed out. In fact, this phenomenon could imply the shrinkage of the spreaded layer and the degradation of polymerised layers surface.

Finally, the deformation of green parts surfaces due to high surface tension must be avoided. The addition

Table 1
Properties of the pure resins

Properties (20 °C)	HDDA	RPCure AR 200	Diacryl 101	SOMOS 6100
Viscosity at 50 s^{-1} (mPa s)	9	980	1800	2460
Density (kg m^{-3})	1030	1207	1120	1150
Refractive index	1.457	–	1.544	1.477

of various surfactants in the UV curable suspensions was considered as a possible solution to this problem.

2. Experimental procedure

2.1. Starting materials

PZT powders were provided with an average size d_{50} of 5 μm. The 10th percentile particle size (d_{10}) of this ceramic was 2.1 μm, and the 90th percentile particle size (d_{90}) was 10.9 μm. Scanning electronic microscopy reveals the irregular shape of the PZT particles. However, as the particles do not seem to have a preferential axis, we will assert their spherical shape for further modelisations. The density of PZT is approximately 7.6 g/cm^3 and their refractive index is 2.5.

Different resins or mixtures of resins were used as liquid medium: on one hand, acrylates (2,2′-bis [4-(methacryloxyethoxy)phenyl]propane called Diacryl 101, Akzo Nobel Chemicals, and 1,6 hexanediol diacrylate called HDDA, UCB) and on the other hand, epoxy or epoxy-acrylates (3,4-epoxycyclohexylmethyl-3,4-epoxycyclohexylcarboxylate trimethylolpropane triacrylate called SOMOS 6100, Dupont and RPCure 200 AR, RPC). The characteristics of the pure resins are shown in Table 1. DMPA (2,2′-dimethoxy-2-phenylacetophenone, Aldrich) was used as UV photoinitiator. To assure a good homogeneity and low viscosity of the high-loaded suspension, the use of a dispersant, acting both by electrostatic and steric repulsion, was compulsory. PZT powder was coated either with stearic acid (for synthesis, Merck) or phosphoric ester.

2.2. Preparation of UV curable suspensions

At first, PZT powder was coated with 1 wt.% dispersant with respect to the ceramic in acetone thanks to an ultrasounds probe (Sonic Dismembrator 550, Fischer Scientific) (Fig. 2). Then the solvent was evaporated at low temperature to allow the dispersant to remain absorbed onto particles surfaces. After drying, PZT was desagglomerated with a 80-μm sieve. Granulometric analyses have demonstrated the absence of aggregates larger than 50 μm. Finally, PZT ceramic was mixed with resin(s) and 1 wt.% photoinitiator by weight of monomer during 40 min by ball milling (300 trs/min) (Retsch PM400, Fischer Scientific).

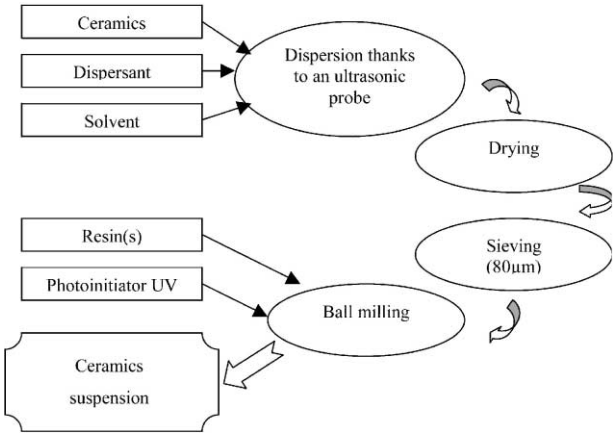

Fig. 2. Preparation of UV curable suspensions of piezoelectric ceramics.

2.3. Characterisation

In this work, rheological measurements were carried out in both steady-state and dynamic regimes.

The viscosity and the rheological behaviour of the suspensions at different fillers contents, surfactant doses and with several resins were measured on a stress-controlled viscometer (CSL-100, Carri-Med) in a cone-plate setting on shear rate range of 0.1–300 s^{-1} at different temperatures. With this kind of configuration, the samples undergo a simple shear deformation. The evolution of stress (τ) as a function of shear rate ($\dot{\gamma}$) characterises the rheological steady state behaviour of the suspension. In steady-state regime, stress and strain rate are related by the following relationship:

$$\tau = \eta \cdot \dot{\gamma}$$

where $\eta = \eta(\dot{\gamma})$ is the sample viscosity.

This viscometer was also used to determine the possible thixotropic character of the ceramic suspensions by successive applications of loading (increasing stress) and unloading (decreasing stress) cycles. A time duration of 30 s was imposed between each stress rise or drop to reveal short time thixotropy effect.

Temperature regulation was ensured by a Peltier-effect plate. Each test was carried out in thermal steady-state.

Creep measurements were performed on CSL-100 viscometer to study viscoelastic behaviour of PZT suspensions. In these tests, a constant stress is applied to the ceramic dispersions and time dependent deformation is recorded. On release of the stress, strain recovery was observed.

Oscillatory experiments were conducted on a stress imposed rheometer (SR 200, Rheometric Scientific). In

dynamic regime, stress and strain can be related as follows:[18]

$$\tau = \overset{*}{G}(\omega)\cdot\gamma$$

where $G*$ is the complex modulus, which can be split in two variables: G', the storage (or elastic) modulus and G'', the loss (or viscous) modulus:

$$\begin{cases} \gamma = \gamma_0 \cdot \overset{i\omega t}{\mathrm{e}} \\ \tau = \tau_0 \cdot \overset{i(\omega t+\delta)}{\mathrm{e}} \\ G*(\omega) = G' + i.G'' \\ G' = \dfrac{\tau_0}{\gamma_0}\cdot\cos\delta \\ G'' = \dfrac{\tau_0}{\gamma_0}\cdot\sin\delta \end{cases}$$

where δ denotes the phase difference between stress and strain. When $G' >> G''$, the suspension is said to have an predominant elastic behaviour; as a contrary, when $G'' >> G'$, viscous behaviour is predominant. The measurements were performed on a 10^{-1}–10^{2} rad s^{-1} frequency range.

Moreover, the colloidal stability of PZT dispersions were investigated by sedimentation rate experiments. The height of clear liquid/turbid liquid interface in test-tubes was monitored visually with time.

Finally, the spreading dynamics of resins on polymerised layers was investigated thanks to a CCD camera.

3. Results and discussion

3.1. The role of dispersants

3.1.1. Dispersant choice

Two dispersing agents were tested during this study: a phosphoric ester (Beycostat C213, CECA) and stearic acid (octadecanoic acid, Merck). The first one is the dispersant usually used in our laboratory for the elaboration of suspensions of fine ceramic powders in organic binders; the second one, was quoted in some litterature articles as being an excellent dispersant.[11,19]

As shown in Fig. 3, the steady state apparent viscosity of the 40 wt.% (10 vol.%) suspensions containing stearic acid is greater than the viscosity of those with phosphoric ester.

The influence of dispersant nature was more distinct through sedimentation experiments (Fig. 4). During sedimentation experiments in test-tubes, a concentration gradient occurs, which generates a diffusion process likely to be opposed to a particle fall. Besides, the terminal velocity of rigid particles is determined by the balance between gravitation forces and friction forces; thus, the particles shape and surface, especially the presence of absorbed dispersant, is essential for the comprehension of this phenomenon. As expected by Kynch theory, sedimentation curves representing the interface height as function of time show a linear behaviour before particles compression. It could be deduced that the sedimentation rate of a 10 vol.% suspension is approximately two times lower with acid stearic than with ester phosphoric as dispersant, respectively, 0.78 and 1.56 mm/h. This order of magnitude is in good agreement with the viscosities measured by the previous rheological experiments: the lower the viscosity is, the greater the sedimentation rate (with acid stearic the viscosity of the suspension is doubled towards ester phosphoric but the terminal velocity of the particles is two times lower).

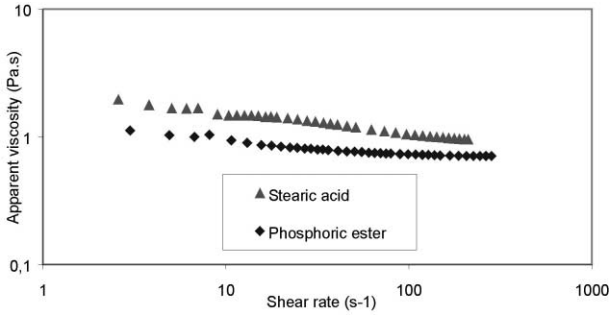

Fig. 3. Influence of dispersant nature on viscosity of 10 vol.% PZT suspensions in HDDA/Somos (17%/83%).

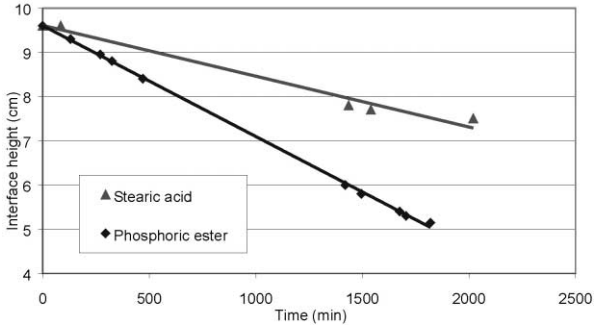

Fig. 4. Determination of sedimentation rate for 10 vol.% PZT dispersions in HDDA/Somos (17%/83%).

In Stokes regime, the diameter d of a sphere isolated in HDDA/Somos (17%/83%) with a 1.56 mm/h terminal velocity is 11 μm:

$$u_t = \frac{g\cdot\left(\rho_s - \rho_f\right)d^2}{18\cdot\eta_f}$$

which leads to

$$d = \left[\frac{18 \cdot u_t \cdot \eta_f}{g.(\rho_s - \rho_f)}\right]^{1/2} = 11 \quad \mu m$$

where u_t is the rate of fall of an unique particle, ρ_s and ρ_f are, respectively, the densities of the solid and the fluid.

It should be stressed that, the average diameter of the sphere obtained with this theory corresponds to the 90th percentile ($d_{90} = 10.9$ μm) of our PZT particles. Thus, the measured sedimentation rates are consistent with the size distribution of our system.

A sedimentation rate of 1.56 mm/h or 0.43 μm/s does not affect seriously the density of the green parts during the process. In fact, the fabrication rate in the vertical direction is 20 μm (a layer) per 20 s, i.e. 1 μm/s, which is slightly greater than the terminal velocity of the PZT particles; particularly because of the re-mixing generate by the motion of the *z*-axis.

In the present work, the phosphoric ester has been chosen as a dispersant because it leads to suspensions owning a lower viscosity and a smoother surface. In fact, suspensions containing stearic acid exhibit foam at their surfaces, which prevent the spreading of homogeneous thin photomaterial layer. In spite of the addition of an antifoaming agent (1-Octanol, Aldrich) the foam remains at the surface of the suspension.

3.1.2. Influence of dispersant concentration

The optimum dispersant concentration was also determined in this study. Fig. 5 shows the influence of dispersant concentration on the samples viscosity. A 1.5% amount of phosphoric ester allows a satisfactory dispersion of the piezoelectric ceramics in the resins and in particular in HDDA. A larger concentration of Beycostat C213 would not bring more consistent benefits on particles dispersion. It could also be noticed that the dispersant concentration has a manifest effect at low shear rates (below 40 s^{-1}) ; an effect which is less distinct at our usual shear rate of processing.

As a result, the dispersant chosen to ensure the stability of the PZT suspensions is the phosphoric ester, with a concentration set at 1.5 wt.% with regard to the PZT weight.

3.2. Rheological behaviour

The steady state rheological behaviour of the suspensions can be modelised by Cross equation:[20]

$$\frac{\eta - \eta_\infty}{\eta_0 - \eta_\infty} = \frac{1}{(1 + (K\dot{\gamma})^m)}$$

where η_0 is the asymptotic value of the viscosity at very low shear rates called low-shear rate Newtonian limit,

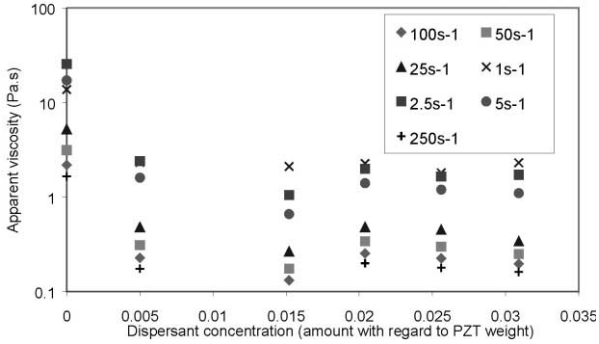

Fig. 5. Influence of dispersant dose on suspension viscosity at various shear rates. Dispersions of 45 vol.% PZT in HDDA.

η_∞ is the high-shear Newtonian limit, K is a constant parameter (in s) and m is a dimensionless index. Thus, at very low shear rates (< 5 s^{-1}), Brownian motion prevails over shearing forces so that the structure of the suspensions is essentially determined by thermal agitation (Fig. 9). The corresponding viscosity is the low-shear rate Newtonian limit. On the contrary, at high shear rates (> 40 s^{-1}), the structure of the dispersion is totally disrupted and the viscosity, called high-shear Newtonian limit η_∞, remains constant (Fig. 10). The intermediate domain of the flow curve, or shear-thinning region, corresponds to the progressive destructuration and orientation of the suspension particles in the shear flow.

In absence of asymptotic stage of the viscosity at very low shear rates, the Cross model reduces to a Sisko model:

$$\tau = \eta_\infty \dot{\gamma} + k\dot{\gamma}^n$$

where k is the consistency in Pa s^n, which can be related to an effective viscosity of the suspensions and n is the power-law index.

In the same way, in absence of asymptotic stage of the viscosity at very low and very high shear rates, the intermediate region can be described by an Ostwald de Waele's "power-law":

$$\tau = k\dot{\gamma}^n$$

The rheological behaviour observed for suspensions with low or medium fillers contents (from 0 to 20 vol.%) have been fitted by Sisko's equation. For suspensions with greater fillers contents, the presence of an asymptotic stage of the viscosity at very low shear rates allows their representations through Cross model (Fig. 9).

In any case, PZT dispersions in monomer resins are fluids that show structural viscosity.

The flexible scrapper used to spread the monomer layers, takes advantage of the shear-thinning behaviour of the suspensions. With an average layer thickness e of

25 μm and a scrapper rate v of 0.5 cm/s, the usual shear rate could be calculated as follows:

$$\dot{\gamma} = v/e = 200 \ \mathrm{s}^{-1}$$

Thus, in this paper, most of the influences on dispersions rheology were studied for high shear rates, principally greater than 40 s^{-1}.

Loading and unloading cycles have revealed the weak thixotropic feature of the samples. Loading curves and unloading ones are superposed, even with a 30 s time between stress rises and drops. Afterwards, thixotropy was neglected in the following experiments.

3.3. Influence of binder nature

Four resins, standard in stereolithography process, were tested with a Carri-Med viscometer. Plastic viscosities for all these photomaterials were ranged between 2.5 and 8.10^{-3} Pa s (Fig. 6). The resin called Somos 6100, composed with epoxy and acrylates groups, has a viscosity too high to be used alone with PZT powder. For instance, a 83 wt.% (45.5 vol.%) PZT suspension with Somos as binder, has a viscosity 100 times higher than the same sample with HDDA as resin. For reactivity and photopolymerisation matters, research focused on two kinds of binders: whether pure HDDA or a mixture of HDDA and Somos. In fact, further works have demonstrated an higher polymerisation depth for PZT suspensions with HDDA/Somos mixture as binder than for other monomers. This is essential to ensure a good connection and cohesion between the photopolymerised layers.

The influence of the proportion of HDDA versus Somos on photomaterial viscosity is shown in Fig. 7. It obeys to the following law:

$$1\mathrm{n}\eta = \Phi_c.1\mathrm{n}\eta_c + (1-\Phi_c).1\mathrm{n}\,\eta\mathrm{d}$$

where Φ_c is the volume fraction of the continuous phase, η_c and η_d are respectively the viscosities of the continuous and the dispersed media.

After polymerisation cure depth measurements, a mixture with 17 wt.% HDDA and 83 wt.% Somos was chosen for further applications. This binder loaded with 45.5 vol.% of piezoceramics reveals a 4.6 Pa s plastic viscosity at 50 s^{-1}, which is rather high for stereolithography applications. As a consequence, this mixture was mostly used for fabrications at low or medium filler contents (up to 23 vol.%). Pure HDDA is the binder for highly loaded suspensions from 23 vol.% to 45.5 vol.% in PZT. It is worth noting that both kinds of dispersions show shear-thinning behaviour.

Observations of resin spreading dynamics have also demonstrated the importance of binder nature. As expected, the addition of HDDA greatly enhances the spreading of monomer layers (Fig. 8).

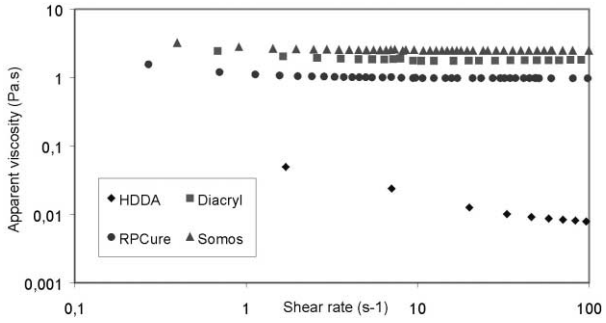

Fig. 6. Flow curves of pure monomers.

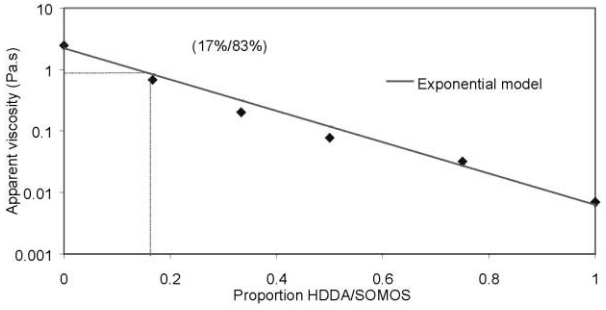

Fig. 7. Influence of resins proportion on binder viscosity.

3.4. Influence of fillers loading

The fabrication of piezoelectric three-dimensional parts requires green parts with a sufficiently high PZT content, in particular if a debinding and sintering cycle is compulsory. However, it was proved in a previous work that light absorption and scattering due to PZT particles lower the cure depth and implies the spreading of thin layers (20 μm).[21]

Thus, it was important to study the effect of solids loading on the flow behaviour of PZT suspensions (Fig. 9). The high-shear Newtonian viscosity, for an HDDA/Somos (17%/83%) suspension with 1 wt.% Beycostat as dispersing agent, has been plotted as a function of ceramic loading (Fig. 10).

As expected, the viscosity of the suspensions increases as the PZT loading increases. A typical curve is shown on Fig. 10 for a 50 s^{-1} shear rate. The viscosity remains low for solid content ranging between 0 and 30 vol.% but undergoes a steep rise at high PZT loadings (>30 vol.%). The viscosity of a 45 vol.% PZT dispersion is 4.8 Pa s, which is rather high for stereolithography purpose.

Different models representing the viscosity of a highly loaded suspension have shown good agreement with these experimental results (Chong, Eilers, Mooney...). The Krieger–Dougherty model also gives a satisfactory estimation of the samples behaviours:

$$\eta = \eta_0 \cdot \left(1 - \beta \cdot \frac{\Phi}{\Phi_0}\right)^{-[\eta]\cdot\Phi_0}$$

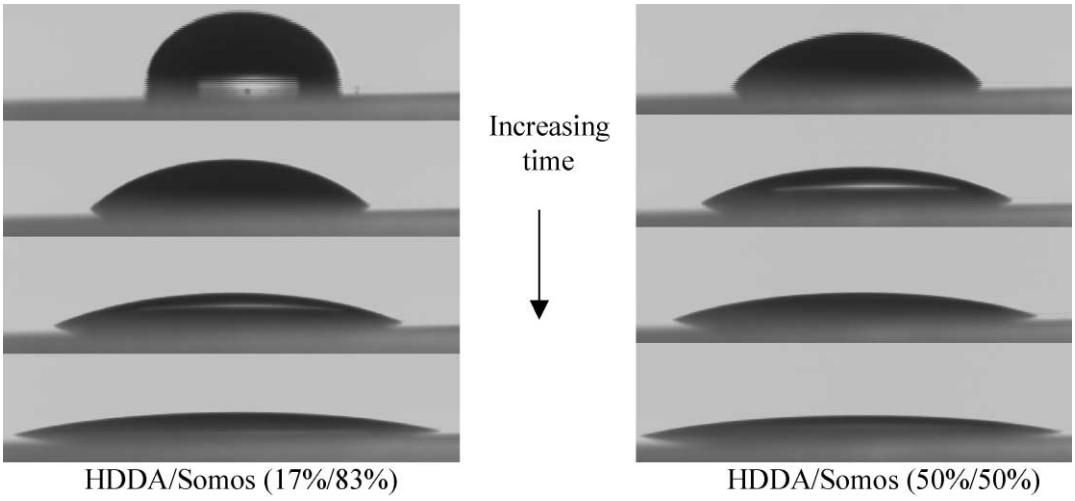

Fig. 8. Spreading dynamics of two photosensitive binders.

in the following relationship, η_0 is the viscosity of the binder and $[\eta]$ is the intrinsic viscosity of the dispersion with $[\eta]=2.5$ for a dilute dispersion of identical rigid spheres. The other variables are the theoretical packing factor Φ_0, which is equal to 0.52 for a cubic simple packing and to 0.64 for random close packing of particles; and the effective packing factor β, which represents the ratio between the volume of a particle with a diameter d coated with dispersant and the same volume without the absorbed dispersant layer:

$$\beta = \left(\frac{d+2b}{d}\right)^3$$

where b is the thickness of the absorbed layer.

A satisfactory fit of the experimental results has been obtained with a packing factor equal to 0.64 and 1.028 for β. As a consequence, the thickness of the phosphoric ester layer was estimated to be $\sim$23 nm at 50 s^{-1}, but this reasoning only takes into account the steric action of the dispersant and not its electrostatic effect. Considering a dispersant with a 16 carbons linear chain, the average quadratic length $\sqrt{r^2}$ of the molecule could be calculated as follows:

$$\sqrt{r^2} = \left(\frac{1-\cos\theta}{1+\cos\theta}\right)^{1/2} \cdot \sqrt{N} \cdot l = 0.84 \text{ nm}$$

where N is the number of segments (15 here), θ is the bonds angle (typically 109.5°) and l the length of a C–C bond (1.54 Å). So, this suggests that the β parameter is not a satisfactory range for an adsorbed layer of a 15-carbons chain, if we only consider steric effect. With phosphoric ester as dispersant, a layer thickness of 23 nm is explainable only if its electrostatic effect is predominant. This result confirms the double effect, electrostatic and steric, of the phosphoric ester.

On the one hand, it should also be pointed out that the value of the consistency of Sisko's law increases

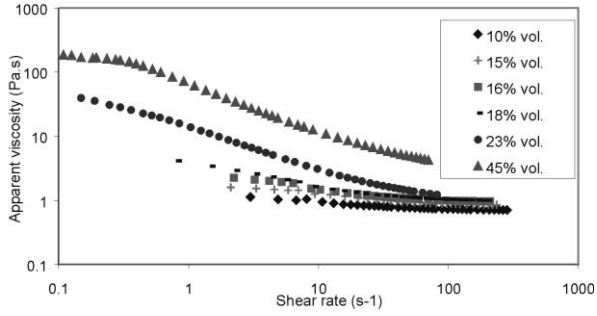

Fig. 9. Apparent viscosity of PZT suspensions near the high-shear Newtonian region ($\dot{\gamma}=50$ s^{-1}).

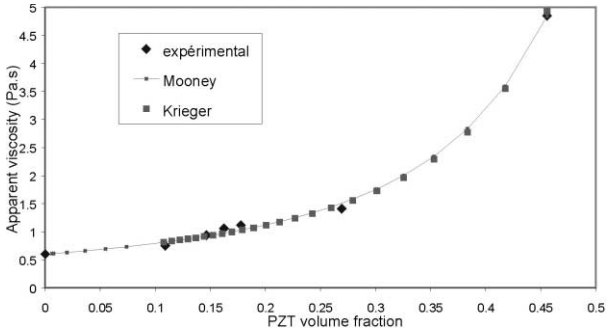

Fig. 10. Influence of fillers content on apparent viscosity.

almost exponentially with the volume fraction of ceramics (Fig. 11). It shows the structuration of the ceramic particles in a dispersion towards the increasing fillers content. On the other hand, the exponent n was found to depend almost linearly on Φ.

The influence of fillers loading was also examined through oscillatory experiments. They reveal a ceramic content threshold comparable to those estimated by Mooney or Chong models and earlier which the suspensions features (viscosity, loss modulus, elastic mod-

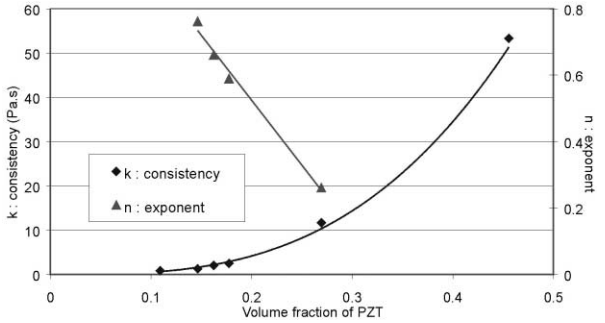

Fig. 11. Influence of fillers content on consisitency index and *n* exponent of Sisko's law.

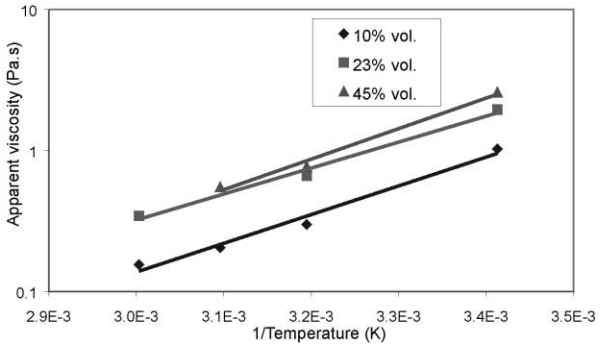

Fig. 12. Temperature dependence of viscosity for different fillers contents.

Table 2
Arrhenius parameters as a function of PZT content in HDDA

Suspensions	HDDA +40% PZT	HDDA +65% PZT	HDDA +83% PZT
A (Pa s)	1.06 E-7	9.66 E-7	1.02 E-7
E_a (J mol^{-1})	39 011	35 255	41 459

ulus) strongly increase with PZT loading. This phenomenon could be related to a percolation threshold.

A solution to compensate for the increase of viscosity due to the introduction of fillers could be the heating of the photomaterials reactor.

PZT dispersions were tested at temperatures ranging from 20 to 60 °C. As expected, a rise of temperature leads to a fall in suspensions viscosities (Fig. 12). Thus, when the temperature increases from 20 to 60 °C, the viscosity of a 65 wt.% (23 vol.%) PZT suspension in HDDA (17 wt.%) and Somos (83 wt.%) decreases from 1.95 to 0.35 Pa s.

An Arrhenius relation can be obtained by plotting the logarithm of the viscosity as function of the inverse of temperature:

$$\eta = A.\exp(\tfrac{E_a}{RT})$$

The activation energy E_a is of the same order of magnitude for all the suspensions, regardless of PZT

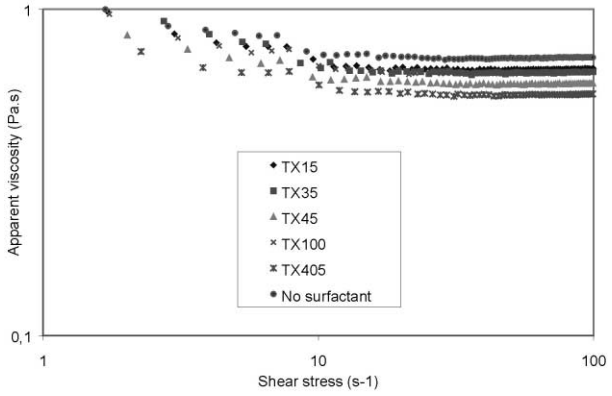

Fig. 13. Influence of surfactant nature (1 wt.%) on binder apparent viscosity.

content (Table 2). This parameter probably depends only on binder nature, because the activation energy of HDDA is approximately 32 000 J mol^{-1}; value which is close to those of PZT suspensions.[15]

Thus, a thermostated reactor is used to compensate the viscosity increase due to high solid loading by a moderate rise of temperature. For instance, with these photomaterials, a 45.5 vol.% PZT dispersion at 38 °C has the same viscosity than a 10 vol.% one at 20 °C.

3.5. Interfacial forces and viscosity: the influence of surfactant content

When a drop of monomer is layed on a polymer surface, it is frequent that the drop does not spread totally on the solid surface but takes a stable position after a transitory deformation. Knowing the surface tension and the contact angle, it is possible to determine the maximum height of the drop thanks to Bashford and Adams equation. Should the drop height be higher than the suspension layer thickness, it would generate layer deformations and, at last, green parts bulging.

In order to improve suspensions spreading and to avoid layer deformations due to high surface tension, different kinds and quantities of surface agents were added to the dispersions. It should be noted that surfactants are widely used to modify surface tension of aqueous solutions but their effects are not proved on such organic resins.

The surfactants are mainly Tritons X (polyethylene glycol ethers for Triton X-100 and X-405, alkylaryl-polyether alcohol: Triton X-45, octyl phenoxy polyethoxyethanol: Triton X-15 and Triton X-35, Rohm and Haas Co.) with different hydrophilic and lipophilic balance (HLB) and also Tween 80 (polyoxyethylene sorbitan monooleate, Sigma-Aldrich) and Span 60 (sorbitan monostearate, Sigma-Aldrich) (Table 3). Fig. 13 shows the influence of surfactant nature on suspension viscosity. Addition of Triton does not seem to change the shape of the rheograms but induces a shift of the

Table 3
HLB of the surfactants

Surfactants	TX-15	Span 60	TX-35	TX-45	TX-100	Tween 80	TX-405
HLB	3.6	4.7	7.8	10.4	13.5	15.0	17.9

curves. As an example, the addition of 1 wt.% TX405, which has the higher HLB, leads to the reduction by 23% of the viscosity.

The effect of concentration is weak compared with other influent parameter and is maximum for approximately 12 wt.% TX405 as displayed in Fig. 14. Unfortunately, as a high density of the green part is requested to improve sintering process, we could not afford using such a concentration of surfactant, the maximum reasonable surface agent content would be 3–5% in weight. It should be noticed that both raw binder and surface agent have higher viscosities than their mixtures.

However, the presence of all these surfactants (from 0.5 to 15 wt.%) does not strongly modify the surface tension of the binder HDDA/Somos (17%/83%), which is 41.5 mN/m. These measurements were made thanks to Wilhelmy strip during pulling out. It should also be stressed that the tested surfactants have few influences on spreading dynamics of these resins.

Thus, the addition of surface agents must be considered only in small proportion to lower viscosities (for some) and not to modify surface tension of such organic binders. In fact, addition of surfactants seems to be inefficient towards interfacial forces. In comparison, for a HDDA/Somos (17%/83%) mixture, the addition of HDDA up to 24% or the augmentation of the temperature by 8 °C would lower the viscosity by 35%, which is more profitable than the addition of 9% TX-405.

3.6. Characterisation of viscoelasticity

Before characterising the viscoelasticity of the suspensions, we should define the behaviours of a linear elastic solid (hookean solid) and of a linear viscous liquid (Newtonian liquid).

A solid is *a material that will not continously change in shape when subjected to a given stress*; if in addition the stress is proportional to the strain, the solid is called "hookean". A fluid is *a material that will continously change its shape when subjected to a given stress, irrespective of how small that stress may be*;[22] if in addition the stress is proportional to the strain, the fluid is called "Newtonian". A viscoelastic fluid possess both viscous and elastic properties. Viscoelastic behaviour is often observed for emulsions or suspensions with high fillers concentrations.[23]

A ceramic suspension with pronounced viscoelastic properties would be embarassing for the fabrication of

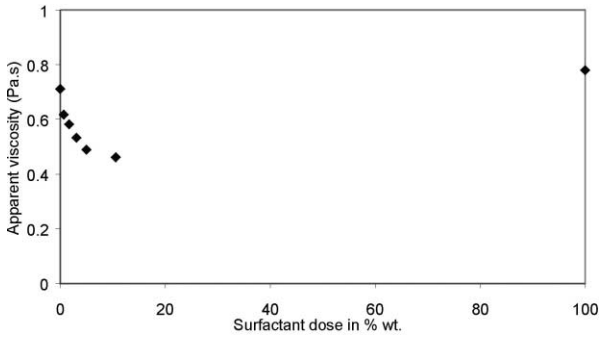

Fig. 14. Binder apparent viscosity as function of TX-405 concentration.

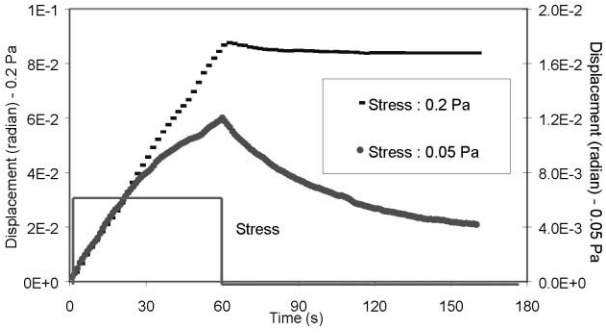

Fig. 15. Creep experiments on 10 vol.% suspension in HDDA/Somos (17%/83%).

PZT green parts by stereolithography process. The shrinkage of the dispersion layer after sweeping by the scrapper, due to viscoelastic phenomenon, could imply the deformation of the three-dimensional part or hinder the layer cohesion.

In order to point out the importance of dispersions viscoelasticity, creep experiments were performed on PZT suspensions (Fig. 15). On the one hand, for an applied stress of 0.2 Pa, the measured displacement remains almost constant when the stress is removed: this behaviour is close to the one of a purely viscous fluid. On the other hand, for an applied stress of 0.05 Pa, the suspension tends to recover its initial position, but a stage is reached for a non-null displacement: this sample demonstrates a viscoelastic behaviour at low applied stresses. Moreover, the measured displacements are null at very short times; so, instantaneous elasticity is excluded.

Stress sweep experiments have been carried out in order to determine the linear viscolelastic domain. As shown on Fig. 16, G'' is approximately stress independent, whereas G' decreases with stress beyond a critical value of 0.15 Pa, which is indicative of the linear range. The drop of G' is due to the destruction of the particles network. This observation is consistent with previous creep experiments (Fig. 15).

Frequency sweep tests were carried out into the linear viscoelastic domain in order to examine the structural

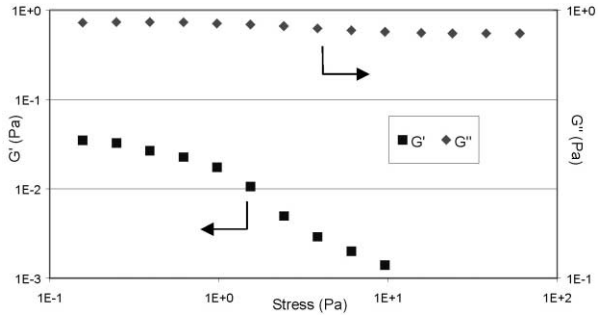

Fig. 16. Stress sweep experiment on 10 vol.% suspension in HDDA/Somos (17%/83%).

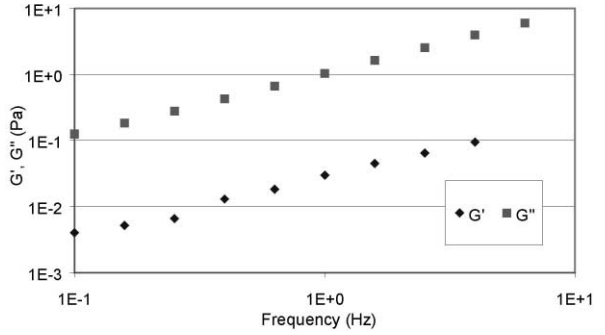

Fig. 17. Determination of elastic and viscous modulus for a 10 vol.% PZT suspension in HDDA/Somos (17%/83%).

rheological characteristics of the samples. The representations of G' and G'' as a function of the frequency show straight lines with slopes with values of 0.9. They have demonstrated the predominance of the viscous modulus (G'') over the elastic one (G'; Fig. 17). Thus, the fluid behaviour is predominant towards to elastic behaviour.

The stress applied during the process being greatly higher than the critical stress of 0.15 Pa (typically 200 Pa), there is no need to take the elastic properties into account. Visually, no significant layer shrinkages were recorded during the fabrication of PZT green parts by stereolithography, even for high fillers content up to 45.5 vol.%.

4. Green parts fabrication

The penetration thickness of the laser is low in the case of PZT powders, comparatively with alumina or silica, which implies a very delicate processing of piezoelectric ceramics by stereolithography.[9,16]

It is necessary to transform the stereolithography process by lowering the deposited layers thickness and by ensuring a good cohesion between the layers. Data files are sliced in 25 or 10 μm layers depending on the desired accuracy.

The weak cure depth on UV irradiation has involved the reduction of the layer thickness down to 25 μm. The

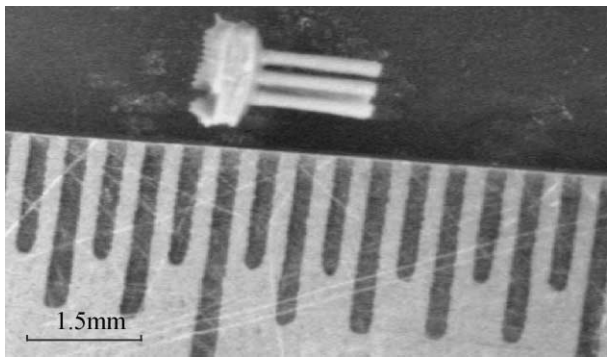

Fig. 18. PZT rods for 1–3 piezocomposites fabrication.

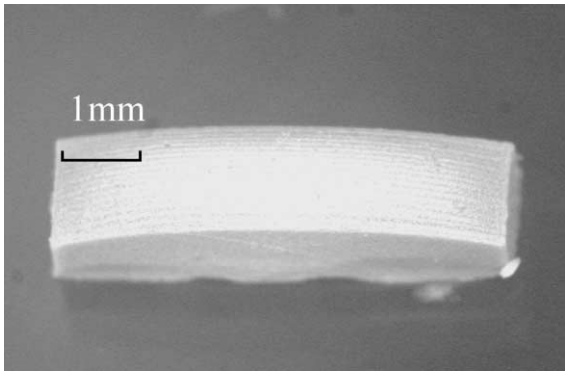

Fig. 19. PZT rods with an high shape factor.

viscosity and the too long spreading time with gravity make the use of a flexible scrapper compulsory. These improvements have led to the design and fabrication of simple green parts with 45.5 vol.% of PZT (Fig. 18) and more elaborated transducers loaded at 15 vol.%, similar in shape to those typically obtain with dice and fill or injection moulding methods (Fig. 19). The piezoelectric properties of the manufactured green parts are studied at present by LPMO laboratory (Besançon). Some of these parts have been sintered at low temperatures (<950 °C) in a lead rich atmosphere. The density of the fired objects is approximately of 7.2 g/cm^3 and the rate of shrinkage (11% for 45.5 vol.% parts) seems to be homogeneous for the three dimensions.

Piezoelectric ceramics/polymer composites with a 1–3 connectivity have shown excellent aptitudes in the domain of medical imaging.[5,6] PZT rods are z-oriented then drowned in an epoxy matrix in order to lower the acoustic impedance of the composites and make it close to human body impedance (1.5 Mrayls). Rods layout, and especially the distance between them, plays a crucial role towards transducers performances and resonance frequencies of the composite. On one hand, the periodicity of the composite structure must be sufficiently fine compared with the plate thickness to favour fundamental

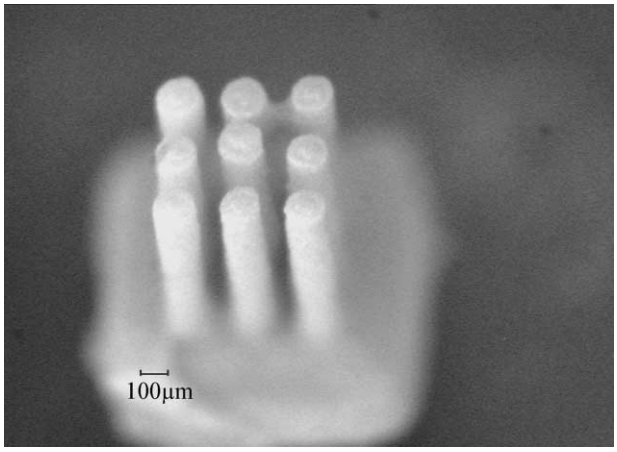

Fig. 20. 45 vol.% PZT transducer.

thickness mode and consider the composite as an homogeneous medium. On the other hand, the distance between rods (or the pitch) is related to the quantity of polymer between them, which allows thickness resonance frequency adjustment. The flexibility of the stereolithography process, with regard to green parts conception and processing, allows the fabrication of three-dimensional parts with a wide range of properties (acoustic impedance, resonant frequency, connectivities...).

Many objects have already been fabricated. They concern especially 1–3 connectivity composites, including rods with 100–300 µm width, height ranging from 0.8–1.5 mm and a 300–100 µm pitch. Figs. 19 and 20 show a three-dimensional part, build with a 25 µm layer thickness, a 100 µm pitch and a form factor (height to width ratio) greater than seven. The characterisation of the piezoelectric properties of such objects are in progress at present.

5. Conclusion

In this paper, the essential influence of ceramic suspensions rheological behaviour towards piezocomposites fabrication by stereolithography was clearly demonstrated.

The study of the influences of the dispersions formulation (binder, surfactant and dispersant natures and amounts), the fillers content and the temperature have led to the choice of two phototsensitive suspensions suitable for stereolithographic purposes: one mixture with 17 wt.% HDDA and 83 wt.% Somos was used for fabrication at low or medium filler contents (up to 23 vol.%), a second one loaded from 23 to 45.5 vol.% in piezoceramics with only HDDA as binder.

Modifications in the stereolithographic process were realised owing to the balance between suspensions rheological and photochemical properties in order to allow piezocomposites fabrication.

Finally, these improvements have led to fabrication of simple green parts with 45.5 vol.% of PZT and more elaborated piezocomposites loaded at 10 vol.% similar in shape to those obtained with other methods. PZT thick films dedicated to transducer applications have also been laid successfully on copper sheets.

Acknowledgements

The authors would like to thank LGEF laboratory (INSA Lyon) for its support and Vincent Mathieu (DCPR) for his assitance in the observation of the spreading behaviour of resins.

References

1. Jaffe, B., Cook, W. R. and Jaffe, H., *Piezoelectric Ceramics*. Academic Press, New York, 1971.
2. Gonnard, P. and Troccaz, M., Matériaux piézoélectriques pour capteurs. *Ann. Chim. Fr.*, 1995, **20**, 383–390.
3. Pilgrim, S. M., Bailey, A. E., Massuda, M., Poppe, F. C. and Ritter, A. P., Fabrication and characterization of PZT multilayer actuators. *Ferroelectrics*, 1994, **160**, 305–316.
4. Panda, R. K. *Fabrication and Properties of Novel PZT Ceramic/Polymer Composites via Solid Freeform Fabrication (SFF) Techniques*. PhD Thesis, Rutgers University, New Brunswick, 2000.
5. Smith, W. A. Composite piezoelectric materials for medical ultrasonic imaging trasnducers—a review. In *Proceedings of the IEEE Ultrasonics Symposium*, 1986, pp. 249–256.
6. Takeuchi, H. and Nakaya, C., PZT/polymer composites for medical ultrasonic probes. *Ferroelectrics*, 1986, **68**, 53–61.
7. Newnham, R. E., Skinner, D. P. and Cross, L. E., Connectivity and piezoelectric-pyroelectric composites. *Mat. Res. Bull.*, 1978, **13**, 525–536.
8. Gururaja, R. T., Schultze, W. A., Cross, L. E. and Newnham, R. E. Ultrasonic properties of piezoelectric PZT rod-polymer composites. In *Proceedings of the IEEE Ultrasonics Symposium*. 1984, pp. 533–538.
9. Chu, G. T. M., Brady, G. A., Miao, W., Halloran, J. W., Hollister, S. J. and Brei, D. Ceramic SFF by direct and indirect stereolithography. In *Solid Freeform and Additive Fabrication MRS Symposium Proceedings*, Vol. 542, 1999, pp. 119–123.
10. Janas, V. F. and Safari, A., Overview of fine-scale piezoelectric ceramic/polymer composite processing. *J. Am. Ceram. Soc.*, 1995, **78**(11), 2945–2955.
11. Lous, G. M., Cornejo, I. A., McNulty, T. F., Safari, A. and Danforth, S., Fabrication of piezoelectric ceramic/polymer composite transducers using fused deposition of ceramics. *J. Am. Ceram. Soc.*, 2000, **83**(1), 124–128.
12. Andre, J. C. and Corbel, S., Stéréophotolithographie Laser. Editions Polytechnica, Paris, 1994.
13. Jacobs, P. F., *Stereolithography and other RP&M Technologies*. Society of Manufacturing Engineers, Dearborn, 1996.
14. Griffith, M. L. Stereolithography of Ceramics. PhD thesis, University of Michigan, 1995.
15. Hinczewski, C., *Stéréolithographie pour la Fabrication de Céramiques*. Thèse de doctorat, Insitut National Polytechnique de Lorraine, 1998.
16. Jang, J. H., Wang, S., Pilgrim, S. M. and Schulze, W. A., Pre-

paration and characterization of barium titanate suspensions for stereolithography. *J. Am. Ceram. Soc.*, 2000, **83**(7), 1804–1806.
17. Chu, G. T. M. and Halloran, J. W., High-temperature flow behavior of ceramic suspensions. *J. Am. Ceram. Soc.*, 2000, **83**(9), 2189–2195.
18. Barnes, H. A., *A Handbook of Elementary Rheology*. Cambrian Printers, Aberystwyth, 2000.
19. Song, J. H. and Evans, J. R. G., Ultrafine ceramic powder injection moulding: the role of dispersants. *Journal of Rheology*, 1996, **40**(1), 131–152.
20. Macosko, W. F., *Rheology. Principles, Measurements, and Applications*. VCH Publishers, New York, 1994.
21. Dufaud, O. and Corbel, S., Stéréolithographie pour la fabrication de composites céramiques piézoélectriques. *Nano et Micro Technologies*, 2001, **1**(2), 177–191.
22. Barnes, H. A., Hutton, J. F. and Walter, K., *An Introduction to rheology*. Elsevier, Amsterdam, 1989.
23. Couarraze, G. and Grossiord, J. L., *Initiation á la Rhéologie*, 1ère édition. Tec & Doc, Lavoisier, 1983.